
Combining mixture models with linear mixing updates: multilayer image segmentation and synthesis

Jonathan Vacher*

Albert Einstein College of Medicine
Dept. of Systems and Comp. Biology
10461 Bronx, NY, USA
jonathan.vacher@einstein.yu.edu

Ruben Coen-Cagli

Albert Einstein College of Medicine
Dept. of Systems and Comp. Biology, and
Dominick P. Purpura Dept. of Neuroscience
10461 Bronx, NY, USA
ruben.coen-cagli@einstein.yu.edu

Abstract

Finite mixture models for clustering can often be improved by adding a regularization that is specific to the topology of the data. For instance, mixtures are common in unsupervised image segmentation, and typically rely on averaging the posterior mixing probabilities of spatially adjacent data points (i.e. smoothing). However, this approach has had limited success with natural images. Here we make three contributions. First, we show that a Dirichlet prior with an appropriate choice of parameters allows – using the Expectation-Maximization approach – to define any linear update rule for the mixing probabilities, including many smoothing regularizations as special cases. Second, we demonstrate how to use this flexible design of the update rule to propagate segmentation information across layers of a deep network, and to train mixtures jointly across layers. Third, we compare the standard Gaussian mixture and the Student-t mixture, which is known to better capture the statistics of low-level visual features. We show that our models achieve competitive performance in natural image segmentation, with the Student-t mixtures reaching state-of-the art on boundaries scores. We also demonstrate how to exploit the resulting multilayer probabilistic generative model to synthesize naturalistic images beyond uniform textures.

1 Introduction

Finite mixture models are a class of unsupervised learning methods that assume the density of observed data is a weighted sum of a parametric template distribution (*e.g.* Gaussian, Exponential, ...). Finite mixture models aggregate data points by their statistical similarity and are widely applied in unsupervised clustering problems [26]. In practice, clustering results are often improved by accounting for the topology of the data [16, 52, 21, 10]. For instance, in image segmentation it is common to encourage the assignment of spatially neighboring pixels to the same cluster, via heuristic spatial smoothing [28, 42] or by augmenting the generative model with *ad-hoc* topology [14, 45]. These approaches however still achieve limited performance in natural image segmentation, compared to state of the art methods based on contour detection [23, 53], and cannot be readily extended to different topologies.

Specifically, in natural images there is a topology associated with the hierarchy of visual features, and segmentation maps based on features at different hierarchical levels could influence (regularize) each other. Studies of human perception have shown that humans are sensitive to segmentation cues at several levels [49, 8, 43, 24, 9], that they can combine segmentation information from multiple levels efficiently [38], and that high level features like objects strongly affect segmentation in human observers [27, 31]. Furthermore, electrophysiology in non-human primates has revealed

*<https://jonathanvacher.github.io>
Preprint. Under review.

that neurons in early and mid-level areas of the visual cortex are sensitive to several segmentation cues [36, 30, 41, 34] and that segmentation information from higher areas influences lower areas via feedback [19, 15].

Approaches based on deep convolutional networks naturally exploit this hierarchical structure, while also often including spatial smoothing, and have thus been extremely successful in the supervised problem of semantic segmentation [22, 37, 6, 2]. Here we leverage the hierarchy of features from a pre-trained network (VGG 19 [44]), and we ask how those could be used to improve unsupervised segmentation based on probabilistic mixture models, and how the resulting multi-layer mixtures can be used to investigate the statistics of deep features and to improve image synthesis.

Contributions To this aim, first we introduce mixture models with Dirichlet prior on the mixing probabilities, and show that an appropriate parametrization of the prior allows us to entirely specify any desired linear update rule for the mixing probabilities, in the EM algorithm. This result includes any form of previously proposed graph Laplacian regularization [16], and further allows us to combine multiple mixture models in a flexible manner through their mixing probability. Second, because this flexible update rule is independent of the parametrization of cluster-specific densities, we can easily compare different likelihood models. The statistics of deep features in natural images have not been fully characterized, but it is expected that superficial layers are sparsely distributed, similar to wavelet coefficients [29, 18], whereas there is some evidence that deeper layers become progressively more Gaussian [39], therefore we compare Gaussian and Student-t mixtures. We test our framework on the BSD 500 [1], and show that although segmentation maps often differ widely across layers, our deep mixtures can encourage consistent segmentations across layers. Quantitatively, we find that the Student-t mixture models achieve state-of-the-art scores on a widely-used boundaries metric, when choosing the best number of components and the best layer. We conclude by showing how to use the fitted mixture models for image synthesis using the deep texture synthesis framework [11].

Notations We use the following notation. Integers H , N and K denote respectively, the number of layers, the number of samples and number of classes/labels. A random variable is denoted by a capital letter X . The probability density function of X is denoted \mathbb{P}_X while x_n denotes a sample. The set Δ^K represents the K -dimensional simplex. A bold letter (lowercase or capital) is a collection of K variables $\mathbf{b} = (b_1, \dots, b_K)$.

2 Mixture Models with Custom Mixing Probabilities Update

We consider a mixture model (1) with Dirichlet prior (2)

$$\mathbb{P}_{X|\mathbf{P}}(x_n|\mathbf{p}_n; \mathbf{a}) = \sum_{k=1}^K p_{n,k} \mathbb{P}_{X^{(k)}}(x_n; a_k), \quad (1) \quad \mathbb{P}_{\mathbf{P}|\mathbf{B}}(\mathbf{p}|\mathbf{b}) = \frac{\Gamma\left(\sum_{k=1}^K b_k\right)}{\prod_{k=1}^K \Gamma(b_k)} \prod_{k=1}^K p_k^{b_k-1}, \quad (2)$$

where $\mathbf{p}_n, \mathbf{p} \in \Delta^K$ are mixing probabilities, \mathbf{a} is the mixture distribution parameter and \mathbf{b} is the Dirichlet prior parameter. The model assumes that the mixing probabilities \mathbf{p}_n depend on the index n of a data sample x_n . As such the mixing probabilities can account for an underlying topology of the dataset $(x_n)_n$ (e.g. when n is attached to a spatial location or a time stamp). The classical Expectation-Maximization (EM) approach consists in completing each sample x_n with a random variable C_n that corresponds to their class. Here, we additionally complete the sample data with another random vector $\mathbf{B}_n \in \mathbb{R}^K$ which will act as a parameter of the Dirichlet distribution. Therefore, we consider $((x_n, C_n, \mathbf{B}_n))_{n \in \{1, \dots, N\}}$ and the completed log-posterior writes

$$\ell(\boldsymbol{\theta}; (x_n, C_n, \mathbf{B}_n)_n) = \sum_{n=1}^N \ln(\mathbb{P}_{\mathbf{P}|\mathbf{B}}(\mathbf{p}_n|\mathbf{B}_n)) + \sum_{k=1}^K \delta_k^{C_n} \left[\ln(p_{n,k}) + \ln(\mathbb{P}_{X^{(k)}}(x_n; a_k)) \right], \quad (3)$$

where $\boldsymbol{\theta} = (\mathbf{p}_n, \mathbf{a})$ and δ_i^j is the Kronecker symbol. The estimation of component parameter \mathbf{a} is independent from the estimation of the mixing probabilities \mathbf{p}_n . It is therefore possible to derive a custom update rule for the mixing probabilities which is applicable to any mixture model as stated in the following proposition.

Proposition 1. For all $(n, k) \in \{1, \dots, N\} \times \{1, \dots, K\}$, let $f_{n,k} : \mathbb{R}^N \rightarrow \mathbb{R}$ be any linear function such that $f_{n,k}([0, +\infty[^N) \subset \mathbb{R}_+$. Set $\mathbf{B}_n = (f_{n,1}(\delta_1^C) - \delta_1^{C_n} + 1, \dots, f_{n,K}(\delta_K^C) - \delta_K^{C_n} + 1)$

as the Dirichlet prior parameter. Then, the mixing probability updates are

$$\forall(n, k) \in \{1, \dots, N\} \times \{1, \dots, K\}, \quad p_{n,k}^{(t+1)} = \frac{f_{n,k}(\tau_{\cdot,k}^{(t)})}{\sum_{k=1}^K f_{n,k}(\tau_{\cdot,k}^{(t)})}. \quad (4)$$

where $\tau_{n,k}^{(t)} = \mathbb{P}_{C_n|X_n, \Theta}(k|x_n, \theta^{(t)})$ is the k^{th} component posterior probability of sample x_n at the previous E-step and $\theta^{(t)}$ is the previous parameter estimate.

Proof. The proof has two steps: (i) take the conditional expectation of the log-posterior (3) knowing the data and the parameters estimated at the last M-step and use the equality $\mathbb{E}((B_{n,k} - 1 + \delta_k^{C_n})|(x_n)_n, \theta^{(t)}) = f_{n,k}(\tau_{\cdot,k}^{(t)})$; (ii) write the Karush–Kuhn–Tucker condition [5] for $p_{n,k}$. See supplementary section A for details. \square

In particular, when $f_{n,k}(\tau_{\cdot,k}) = \sum_m \tau_{m,k}$, the update corresponds to the standard mixture model. When $f_{n,k}(\tau_{\cdot,k}) = \tau_{n,k}$, the mixing probabilities will be equal to the component posterior probability of x_n . Finally, when $f_{n,k}(\tau_{\cdot,k}) = K * \tau_{\cdot,k}|_n$ where K is any averaging kernel and $*$ is a convolution operator, both adapted to the topology of indexes n , the update corresponds to a local average of the posterior as has been used recently for spatial smoothing [46, 16].

The graphical representation of the proposed mixture models 1b has an additional node compared to the graph of the standard mixture models 1a. Note that the loop in the graphical model complicates full inference. However, in practice, we perform only a partial inference: variables \mathbf{a} and \mathbf{P} are inferred (M-step) while variables C and B are estimated by posterior expectation (E-step). Alternatively, to avoid such a loop, it is possible to restrict the variables $B_{n,k}$ to depend only on contextual points (*i.e.* excluding n), yet this leads to similar results in our application. Proposition 1 allows to simplify the graphical representation 1b because \mathbf{B} is a deterministic function of C which can be represented as an undirected edge between \mathbf{P} and C , see 1c.

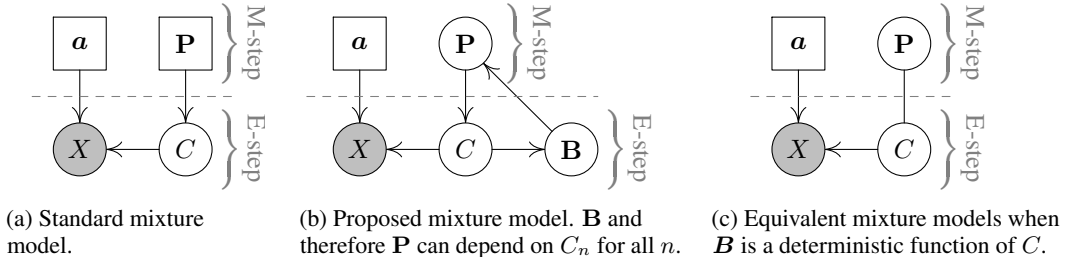


Figure 1: Change in the graphical representation of the mixture models. Index n is omitted for variables X , C , \mathbf{B} and \mathbf{P} .

3 Multilayer Mixture Model for Image Segmentation and Synthesis

3.1 Learning Probabilistic Segmentation Maps using Mixture Models

To tackle multilayer image segmentation with mixture models, we assume that a collection of feature vectors $(x_n^{(h)})_{h \in \{1, \dots, H\}}$ is associated with a pixel n at location $l_n \in \mathbb{L}$ where \mathbb{L} denotes the image lattice. The index h denotes a layer and different layers represent features that are different in nature *i.e.* that are not directly comparable. We assume that an ideal observer learns, at each layer $h \in \{1, \dots, H\}$, a probabilistic map $\hat{\mathbf{p}}_n^{(h)} = \hat{\mathbf{p}}^{(h)}(l_n)$ (and also mixture parameters $\hat{\mathbf{a}}^{(h)}$) which are mixing probabilities of a mixture model. Inference is achieved by maximum a posteriori estimation

$$(\hat{\mathbf{a}}, \hat{\mathbf{p}}) = \operatorname{argmax}_{(\mathbf{a}, \mathbf{p})} \sum_{n=1}^N \ln (\mathbb{P}_{\mathbf{A}, \mathbf{P}(l_n)|X, C, \mathbf{B}}(\mathbf{a}, \mathbf{p}(l_n)|x_n, C(l_n), \mathbf{B}(l_n))), \quad (5)$$

where we dropped the dependence on h because all variables depend on h . The posterior in Equation (5) is obtained using the Bayes theorem as the combination of the mixture model (1) that accounts

for local image statistics and the Dirichlet prior (2) that accounts for the hierarchical local grouping. For a feature vector x associated with location l ,

$$\mathbb{P}_{\mathbf{A}, \mathbf{P}^{(l)} | X, C^{(l)}, \mathbf{B}^{(l)}}(\mathbf{a}, \mathbf{p}^{(l)} | x, C^{(l)}, \mathbf{B}^{(l)}) \propto \underbrace{\mathbb{P}_{X, C^{(l)} | \mathbf{A}, \mathbf{P}^{(l)}}(x, C^{(l)} | \mathbf{a}, \mathbf{p}^{(l)})}_{\text{local image statistics}} \underbrace{\mathbb{P}_{\mathbf{P}^{(l)} | \mathbf{B}^{(l)}}(\mathbf{p}^{(l)} | \mathbf{B}^{(l)})}_{\text{hierarchical local grouping}}.$$

The proposed custom mixture model offers a flexible framework to combine the multiple layers using the Dirichlet prior on the probability maps. In Proposition 1, \mathbf{B}_n is a function of C , here $\mathbf{B}^{(h)}(l_n)$ is a function of $(C^{(1)}, \dots, C^{(H)})$ i.e. it will regularize the mixing probability $\mathbf{p}^{(h)}(l_n)$ with the knowledge of the class in the neighboring pixels and layers. First, we consider that layers are independent (Figure 2a), second, that all layers share the same prior probability maps (Figure 2b) and third, that the prior probability maps of each layer accounts for the classes of the previous and next layers (Figure 2c).

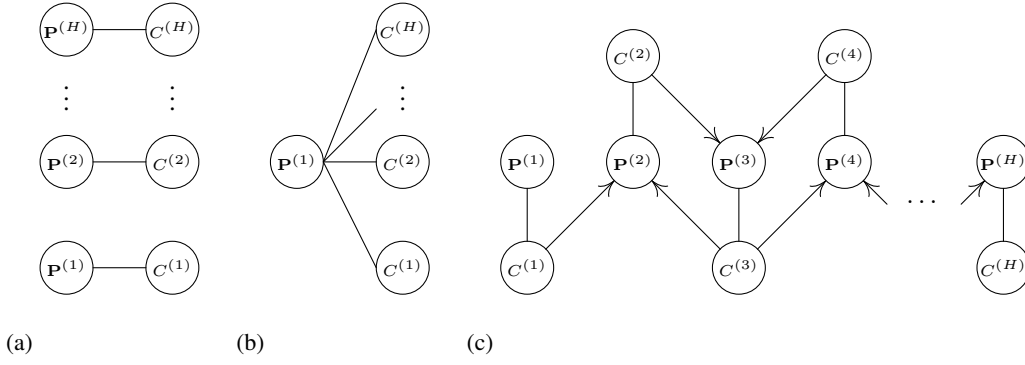


Figure 2: Graphical representations of the proposed multilayer mixtures. We only represent connections between \mathbf{P} and C , yet C has an implicitly directed connection to X which receives a directed connection from \mathbf{a} (see figure 1c). Index n is omitted.

By choosing $\mathbf{B}^{(h)}(l_n)$ appropriately (see supplementary section A, Proposition 3), the three models have respectively the following update rules for all $h \in \{1, \dots, H\}$,

$$p_{n,k}^{(h,t+1)} = \frac{s_n^{(h,t)^2} \tau_{n,k}^{(h,t)} + m_{n,k}^{(h,t)}}{s_n^{(h,t)^2} + 1}, \quad (6) \quad p_{n,k}^{(1,t+1)} = \frac{\sum_{h=1}^H \prod_{i \neq h} s_n^{(i,t)^2} m_{n,k}^{(h,t)}}{\sum_{h=1}^H \prod_{i \neq h} s_n^{(i,t)^2}}, \quad (7)$$

$$p_{n,k}^{(h,t+1)} = \frac{s_n^{(h,t)^2} s_n^{(h+1,t)^2} m_{n,k}^{(h-1,t)} + s_n^{(h-1,t)^2} s_n^{(h+1,t)^2} m_{n,k}^{(h,t)} + s_n^{(h-1,t)^2} s_n^{(h,t)^2} m_{n,k}^{(h+1,t)}}{s_n^{(h,t)^2} s_n^{(h+1,t)^2} + s_n^{(h-1,t)^2} s_n^{(h+1,t)^2} + s_n^{(h-1,t)^2} s_n^{(h,t)^2}}, \quad (8)$$

where

$$m_{n,k}^{(h,t)} = G^{(h)} * \tau_k^{(h,t)}(l_n), \quad (9) \quad s_n^{(h,t)^2} = \frac{\sum_{k=1}^K G^{(h)} * \tau_k^{(h,t)^2}(l_n) - m_{n,k}^{(h,t)^2}}{K(1 - G * G(0))}, \quad (10)$$

are respectively the local mean and variance of the posterior maps at layer h , $\tau_k^{(h,t)} : l_n \mapsto \tau_{n,k}^{(h,t)}$ is the posterior maps at layer h and $G^{(h)}$ is a Gaussian kernel with width $\sigma^{(h)}$. As such, these updates correspond to the sum of local evidence in each layer (local pixel statistics) weighted by their uncertainty. The first update combines local ($m_{n,k}^{(h,t)}$) and single pixel ($\tau_{n,k}^{(h,t)}$) evidence from independent layers in independent collections of mixing probability maps $(\mathbf{p}_n^{(h)})_{n,h}$. The second update combines all local evidence ($m_{n,k}^{(h,t)}$) from all layers h in a single collection of mixing probability maps $(\mathbf{p}_n^{(1)})_n$, therefore enforcing consistent segmentation for all layers. Finally, the third update combines local evidences from current ($m_{n,k}^{(h,t)}$), previous ($m_{n,k}^{(h-1,t)}$) and next layers ($m_{n,k}^{(h+1,t)}$) in collections of mixing probability maps $(\mathbf{p}_n^{(h)})_{n,h}$, thus encouraging consistent segmentation for

adjacent layers. The single pixel evidence term $\tau_{n,k}^{(h,t)}$ is removed in updates (7) and (8) because its weights will always be one order of magnitude smaller than other terms.

The three models 2a,2b and 2c are fitted by running H EM algorithms with respectively the modified update rule 6,7 and 8. See algorithm 1 for pseudo code.

3.2 Image Synthesis from Mixtures

The proposed multilayer mixture models capture the statistics of image features at each layer, inside each segment (component), and thus represent generative models of those features. Therefore, to synthesize images, a direct approach would be to sample features values from the learned mixture components at all layers and segments, and then modify the pixels of a white noise image (the seed) by minimizing the mean squared error between the sampled features and the features of the seed image.

This approach however does not converge to anything resembling a natural image, because our models do not account for the fact that features at one layer are computed from the previous layer (in other words, in the generative model there are no dependencies between features across layers, only between segmentations). To preserve the relations between layers, we propose a variant of the deep texture synthesis algorithm introduced by Gatys *et al.* [11]: we enforce the statistics of the deep features of the seed image to be close the statistics of a target natural image, at each layer and within each segment. Specifically, we define the following loss function, and minimize it with respect to the pixels of the seed image using back-propagation

Algorithm 1: Algorithm for models 2b/2c.

Input : Number of iteration n_{iter} , of components K , of layers H , kernel widths $(\sigma^{(h)})_h$ and data $(x_n^{(h)})_{n,h}$.

Output : Mixing probability maps $\hat{\mathbf{p}}^{(h)}$ and mixture parameters $\hat{\mathbf{a}}^{(h)}$.

Initialize mixture parameters of layer 1 with K-means algorithm. Initialize mixing probabilities of other layers with the posterior probabilities of layer 1.

Run M-step for all layer $h \geq 2$.

for $t = 1$ **to** n_{iter} **do**

for $h = 1$ **to** H **do**

 E-step: compute $\tau_k^{(h,t)}$.

end

for $h = 1$ **to** H **do**

 M-step:

 - compute mixing probability maps $p_{n,k}^{(h,t+1)}$ using Equation (7) or (8),

 - compute model parameter $\mathbf{a}^{(h,t+1)}$.

end

end

$$\mathcal{L}(x^{(0)}) = \sum_{h=1}^{\bar{H}} \sum_{k=1}^K \left\| \text{Ave}_k^{(h)}(x^{(0)}) - M_k^{(h)} \right\|^2 + \left\| \text{Cov}_k^{(h)}(x^{(0)}) - C_k^{(h)} \right\|^2 \quad (11)$$

where $\text{Ave}_k^{(h)}$ (resp. $M_k^{(h)}$) and $\text{Cov}_k^{(h)}$ (resp. $C_k^{(h)}$) are the empirical mean and covariance of segment k at layer h of the deep features of the seed image $x^{(0)}$ (resp. the target image).

In this paper, we limit ourselves to enforce the means and covariances, but future work could include also the Student-t scale parameter, or use optimal transport theory to directly adjust features to the desired distributions [13, 12]. Importantly, in Equation (11) the statistics are computed within each segment, and incompatible segmentations across layers could in principle produce conflicts in the optimization. Our models 2b and 2c offer two ways to enforce consistency across layers. In practice, we find that the color space of the synthesized image often appears different from the target; this is corrected by color histogram matching using sliced Wasserstein projections [3].

4 Results

Segmentation We test the three models presented in section 3 using Gaussian mixture models (GMM) and Student-t mixture models (SMM) with image deep features obtained with the pre-trained deep network VGG 19 [44]. See [26] and references therein for complete EM algorithms. We use Gaussian distributions because they are a popular choice for finite mixtures, and the Student-t distributions because it captures better the sparse, heavy-tailed behavior of low-level features in

natural images [50, 39]. To quantify natural image segmentation performances, we use three widely-adopted scores: the adjusted Rand Index (aRI) [17], the F-score for boundaries (F_b) and for objects and parts (F_{op}) [32].

Applying the framework described in section 3 requires few elaborations. First, the number of pixels (*i.e.* the number of samples) is not same in the different layers, therefore we up-sample the posterior probability maps $\tau_k^{(h,t)}$ using nearest neighbor interpolation before the convolution with kernel $G^{(h)}$ when it is necessary. Second, the decreasing number of samples and the increasing dimension of features along the depth of the network often causes numerical issues, therefore we reduce the dimension at each layer using Principal Component Analysis (PCA) to capture 90% of the variance. Third, the first layer of the deep network is a linear transform of the input image in contrast with all subsequent layers, therefore we add the features of the first layer to all subsequent layers (using average pooling when necessary). We run the algorithms with the following values of $\sigma^{(h)}$: 4.25, 4.25, 3.25, 3.25, 2.25, 2.25, 2.25, 2.25, 0.75, \dots , 0.75 for models 2a and 2c and 2.25, 2.25, 1.75, 1.75, 1.25, 1.25, 1.25, 1.25, 0.75, \dots , 0.75. for model 2b. Quantitative results are summarized in Figure 3, using the number of components K that gives the maximal score. First, all three scores share a similar trend associated with the considered mixture model. For SMM, the average scores decrease from superficial to deep layers (with the exception of aRI with model 2c which is marginally increasing after layer 10). These decreases are due to the reduction in resolution with the increasing depth (see supplementary Figure 7). The decrease is linear and more pronounced for F_b than for aRI, while it is decreasing in three steps for F_{op} (layer 1-8, layer 9-12 and layer 13-16). These differences may arise because accurate contour detection (F_b) requires more resolution than region identification (aRI and F_{op}). For GMM, the scores are slightly decreasing between layers 1 and 4 to reach a plateau between layers 5 and 9. Then, aRI and F_b jump up and fill the gap with the SMM scores. The trend is similar but weaker in F_{op} . Together, these trends suggest that deep features initially become less Gaussian before being more Gaussian in the deepest layers. This contrasts with Sanchez *et al.* [39] where Gaussianity is proposed to increase monotonically along the depth of the network. Yet, our measures are segmentation-based and results from single-image statistics. For example, the similar performance of GMM and SMM in deep, low-resolution layers may reflect that there are not enough samples to accurately fit the Student-t distributions.

Second, for SMM, we observe that model 2c often increases the layers-wise scores obtained with model 2a, particularly in the deep layers, where model 2c can use information from the higher resolution layers. In contrast for GMM, model 2c decreases the scores obtained with model 2a up to layers 11 (aRI) and 7 (F_b). Overall, the trends in F_{op} are less clear because of the large error bars. The scores obtained for model 2b are similar to the maximal average scores over all layers. For models 2a and 2c, choosing the maximal score obtained among layers per image often increases the overall performance for all scores (Figure 3 right). In particular, SMM reaches state-of-the-art performance for F_b . These results indicates that the simple proposed layer combination 2b is too simplistic to increase the overall

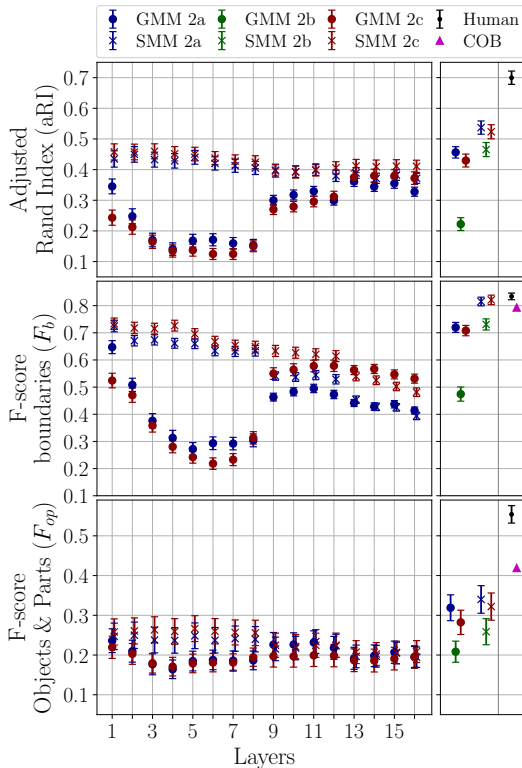


Figure 3: Results on the BSD 500 for the three scores referred in text. Left: results for each layer for models 2a and 2c averaged over the BSD (with best number of components K per image). Right: results averaged over the BSD (with best number of components K and best layer h per image). COB refers to the algorithm presented in [23]. Error bars indicates 3 standard error of the mean.

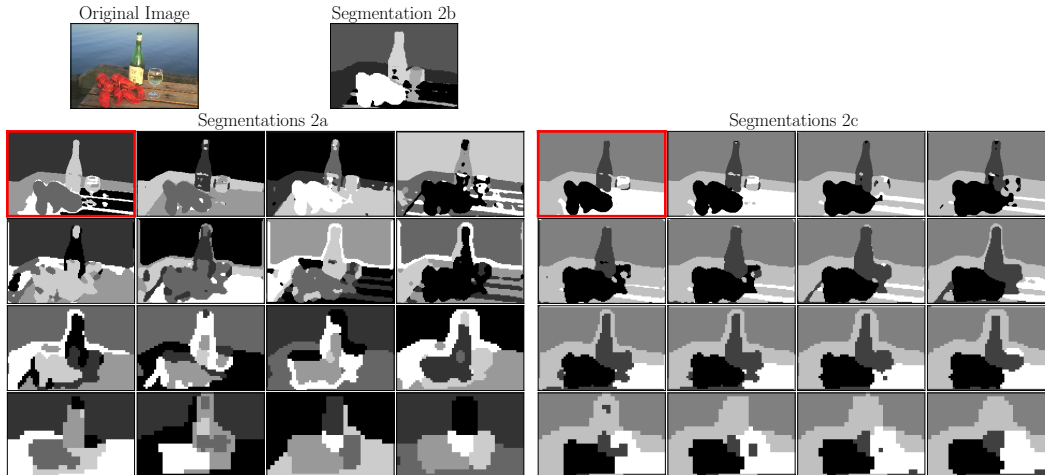


Figure 4: Segmentation maps obtained with Student- t mixtures for the three models. All layers have the same number of components corresponding to the number of components of the best layer. The red frame indicates the best layer (highest aRI score).

segmentation performances obtained without layer combination (model 2a). In addition, while the layer combination 2c consistently increases all scores at all layers, there are only marginal changes when the best layer is selected per image. This could be explained because by enforcing consistency between segmentation maps, model 2c reduces their diversity and therefore the possibility to have better segmentation maps among the layers as it is the case for model 2a.

Figure 4 shows segmentation maps with the same number of components at all layers with SMM on one image. Model 2a highlights that different layers result in different segmentation maps. For example, in layers 6-8 the border between wood and water is a proper segment in contrast to other layers. Model 2c has the advantage to make segmentation coherent across layers reducing segmentation variability between layers. Model 2b has the advantage of combining knowledge between all layers avoiding the choice of the best layer. Figure 5 illustrates that the best number of components varies across layers.

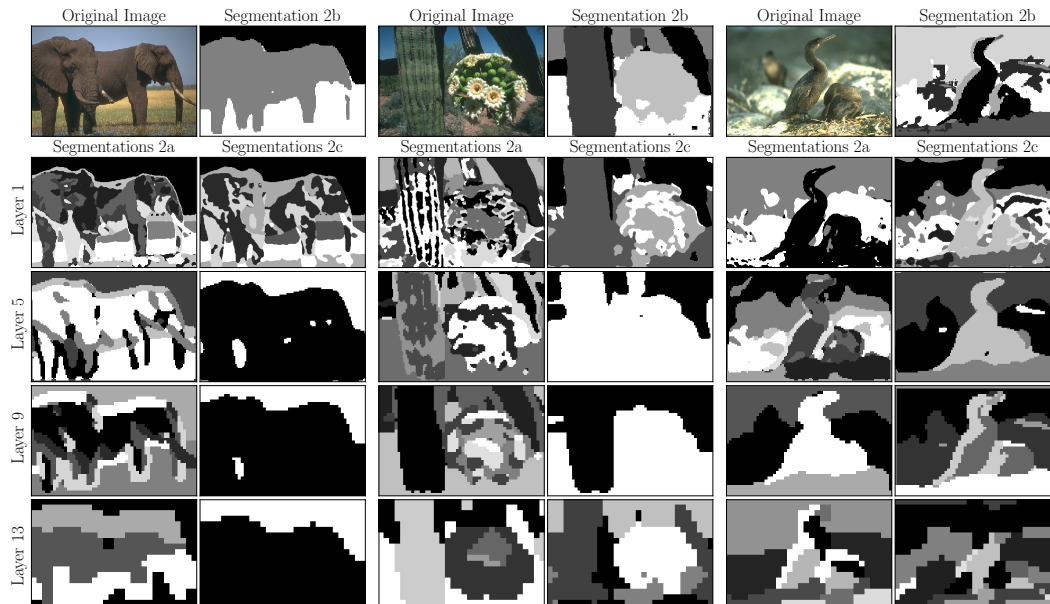


Figure 5: Segmentation maps obtained with Student- t mixtures for the three models. For each layer we show the number of components that gives the best aRI score for that layer.

Image synthesis Beyond capturing segmentation maps, our multilayer mixture models also capture the statistics of the contents of each segment at each layer. Therefore the resulting segmentations can

guide the synthesis of naturalistic images as a collage of textures that match the statistics inside each segment at each layer, as detailed in section 3. Figure 6 demonstrate the feasibility of this approach, using the SMM with model 2c) to encourage consistent segmentations across layers. As expected the fine details inside each segment are lost and replaced by textures, but the overall image composition is preserved. This approach to synthesis can be applied and extended to address several interesting questions. First, enforcing different levels of consistency across layers would allow us to explore the effect of segmentation inconsistency on image appearance. Second, we find for the example images that to achieve good quality synthesis we need to capture more variance (*i.e.* more dimension) at each layer ($\geq 99\%$), compared to segmentation. This could be because few dimensions are sufficient to discriminate segments in an image, but more are required to fully capture their natural appearance. We hypothesize that the different textures composing images do not lie in a common low dimensional sub-space, but in multiple low dimensional linear sub-spaces. Lastly, we speculate that these synthetic images would be indistinguishable from natural images in peripheral vision [51], and therefore the proposed synthesis method could be readily applied to study perceptual segmentation in humans.

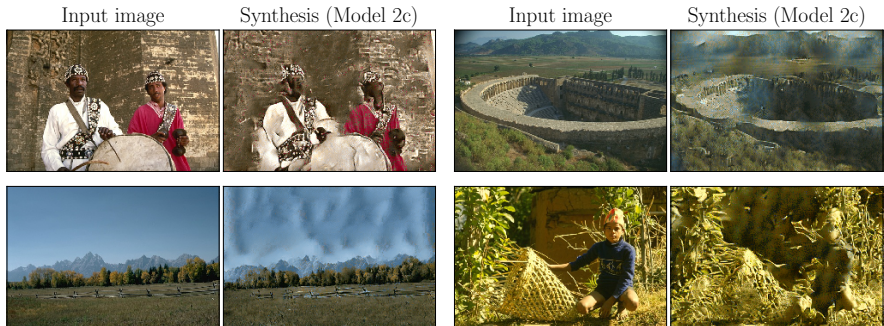


Figure 6: *Examples of image synthesis using the five first layers (see the segmentation maps used for synthesis in supplementary Figures 8–11). Left: good synthesis. Right: bad synthesis.*

5 Discussion

We propose a flexible extension to mixture models that allows to choose any linear update rule for the mixing probabilities in the EM algorithm. We empirically observe the likelihood to increase at each step as it is the case for the classical EM algorithm. While, we do not provide any proof of convergence, no further elaborations are required in the standard proof of EM convergence to prove convergence to a local minimum of the proposed mixture model [25].

The subsequent proposed multilayer combination differs from previously proposed deep GMMs [48, 47]. First, it applies to any kind of mixture models, and second it does not learn a multilayer representation but instead it aims at capturing the statistics of an existing multilayer representation. In addition it affords full flexibility in how to combine different layers.

Our results show that mixture models could achieve state of the art on boundary F-score. Yet, this requires using the ground-truth (human) segmentation maps to select the layer and number of components that maximized the scores. Furthermore, the three scores often lead to different choices for the best layers and the best number of components. A better model requires automatic selection of these two variables, which could be achieved using the Bayesian Information Criterion [26] or by multiplying the mixing probabilities \mathbf{p}_n by a single Dirichlet vector \mathbf{q} with parameters that favor sparsity [35].

We also propose an image synthesis algorithm that exploits our multilayer mixture models, and demonstrate how synthesis can be an important complement to segmentation to assess the quality of such models. We also observe that dimensionality reduction can be effective for segmentation but it is limited to achieve good synthesis. Possible improvement in segmentation and synthesis could be achieved by using more involved mixture models such as subspace clustering methods [4] which can find the right low-dimensional subspace for each mixture component (see section 4 end of image synthesis paragraph).

The present work also offers insights into natural images statistics and their role in biological vision. First, assuming Gaussian distributions for the features of deep networks leads to worse segmentation,

compared to Student-t, for superficial layers, but similar performance for deeper layers. This is broadly consistent with the known sparsity of low-level features [50] and with the recent observation that deeper layers are more Gaussian [39], and illustrates the functional consequence of accounting for those statistics. Second, similar to our model, different visual-cortical areas convey information about different features. Our multilayer segmentations could be used to probe segmentation in different cortical areas. In addition, in line with previous work in low-level vision [20] and more broadly with the theory of probabilistic inference in the brain [33], our methods to combine these maps by accounting for their uncertainties could inform studies of cortical feedback. The models could also be extended to include other influences like environmental context or task-oriented attention (e.g. visual search).

The proposed segmentation models rely on the use of the introduced flexible mixture models. There is no indications of what could physiologically account for the mixing probabilities. A possible alternative is to formulate explicitly the Student-t mixture models as mixtures of Gaussian scale mixtures, which explain neural activity in visual cortex [7]. In such double mixture models, it should be possible to apply the smoothing regularization not on the mixing probabilities but on the scale mixers [7, 40].

References

- [1] Pablo Arbelaez, Michael Maire, Charless Fowlkes, and Jitendra Malik. Contour detection and hierarchical image segmentation. *IEEE transactions on pattern analysis and machine intelligence*, 33(5):898–916, 2011.
- [2] Vijay Badrinarayanan, Alex Kendall, and Roberto Cipolla. Segnet: A deep convolutional encoder-decoder architecture for image segmentation. *IEEE transactions on pattern analysis and machine intelligence*, 39(12):2481–2495, 2017.
- [3] Nicolas Bonneel, Julien Rabin, Gabriel Peyré, and Hanspeter Pfister. Sliced and radon wasserstein barycenters of measures. *Journal of Mathematical Imaging and Vision*, 51(1):22–45, 2015.
- [4] Charles Bouveyron and Camille Brunet-Saumard. Model-based clustering of high-dimensional data: A review. *Computational Statistics & Data Analysis*, 71:52–78, 2014.
- [5] Stephen Boyd and Lieven Vandenberghe. *Convex Optimization*. Cambridge University Press, 2004.
- [6] Liang-Chieh Chen, George Papandreou, Iasonas Kokkinos, Kevin Murphy, and Alan L Yuille. Deeplab: Semantic image segmentation with deep convolutional nets, atrous convolution, and fully connected crfs. *IEEE transactions on pattern analysis and machine intelligence*, 40(4):834–848, 2018.
- [7] Ruben Coen-Cagli, Adam Kohn, and Odelia Schwartz. Flexible gating of contextual influences in natural vision. *Nature Neuroscience*, 18(11):1648, 2015.
- [8] James H Elder and Richard M Goldberg. Ecological statistics of gestalt laws for the perceptual organization of contours. *Journal of Vision*, 2(4):5–5, 2002.
- [9] Charless C Fowlkes, David R Martin, and Jitendra Malik. Local figure–ground cues are valid for natural images. *Journal of Vision*, 7(8):2–2, 2007.
- [10] Haitao Gan, Nong Sang, and Rui Huang. Manifold regularized semi-supervised gaussian mixture model. *JOSA A*, 32(4):566–575, 2015.
- [11] Leon Gatys, Alexander S Ecker, and Matthias Bethge. Texture synthesis using convolutional neural networks. In *Advances in Neural Information Processing Systems*, pages 262–270, 2015.
- [12] Aude Genevay, Marco Cuturi, Gabriel Peyré, and Francis Bach. Stochastic optimization for large-scale optimal transport. In D. D. Lee, M. Sugiyama, U. V. Luxburg, I. Guyon, and R. Garnett, editors, *Advances in Neural Information Processing Systems 29*, pages 3440–3448. Curran Associates, Inc., 2016.
- [13] Aude Genevay, Gabriel Peyré, and Marco Cuturi. Learning Generative Models with Sinkhorn Divergences. *arXiv e-prints*, page arXiv:1706.00292, Jun 2017.
- [14] Soumya Ghosh, Andrei B Ungureanu, Erik B Sudderth, and David M Blei. Spatial distance dependent chinese restaurant processes for image segmentation. In *Advances in Neural Information Processing Systems*, pages 1476–1484, 2011.

- [15] Charles D Gilbert and Wu Li. Top-down influences on visual processing. *Nature Reviews Neuroscience*, 14(5):350, 2013.
- [16] Xiaofei He, Deng Cai, Yuanlong Shao, Hujun Bao, and Jiawei Han. Laplacian regularized gaussian mixture model for data clustering. *IEEE Transactions on Knowledge and Data Engineering*, 23(9):1406–1418, 2010.
- [17] L. Hubert and P. Arabie. Comparing partitions. *Journal of classification*, 2(1):193–218, 1985.
- [18] Aapo Hyvärinen, Jarmo Hurri, and Patrik O Hoyer. *Natural image statistics: a probabilistic approach to early computational vision*. Springer.
- [19] P Christiaan Klink, Bruno Dagnino, Marie-Alice Gariel-Mathis, and Pieter R Roelfsema. Distinct feedforward and feedback effects of microstimulation in visual cortex reveal neural mechanisms of texture segregation. *Neuron*, 95(1):209–220, 2017.
- [20] Michael S. Landy and Hiroyuki Kojima. Ideal cue combination for localizing texture-defined edges. *Journal of the Optical Society of America. A, Optics, image science, and vision*, 18 9:2307–20, 2001.
- [21] Jialu Liu, Deng Cai, and Xiaofei He. Gaussian mixture model with local consistency. In *Twenty-Fourth AAAI Conference on Artificial Intelligence*, 2010.
- [22] Jonathan Long, Evan Shelhamer, and Trevor Darrell. Fully convolutional networks for semantic segmentation. In *Proceedings of the IEEE conference on computer vision and pattern recognition*, pages 3431–3440, 2015.
- [23] Kevis-Kokitsi Maninis, Jordi Pont-Tuset, Pablo Arbeláez, and Luc Van Gool. Convolutional oriented boundaries: From image segmentation to high-level tasks. *IEEE transactions on pattern analysis and machine intelligence*, 40(4):819–833, 2018.
- [24] David R Martin, Charless C Fowlkes, and Jitendra Malik. Learning to detect natural image boundaries using local brightness, color, and texture cues. *IEEE Transactions on Pattern Analysis & Machine Intelligence*, (5):530–549, 2004.
- [25] Geoffrey J. McLachlan and Thriyambakam Krishnan. *The EM algorithm and extensions*. Wiley series in probability and statistics. Wiley, Hoboken, NJ, 2. ed edition, 2008.
- [26] Geoffrey J McLachlan, Sharon X Lee, and Suren I Rathnayake. Finite mixture models. *Annual review of statistics and its application*, 6:355–378, 2019.
- [27] Peter Neri. Object segmentation controls image reconstruction from natural scenes. *PLoS biology*, 15(8):e1002611, 2017.
- [28] Christophoros Nikou, Aristidis C Likas, and Nikolaos P Galatsanos. A bayesian framework for image segmentation with spatially varying mixtures. *IEEE Transactions on Image Processing*, 19(9):2278–2289, 2010.
- [29] Bruno A Olshausen and David J Field. Emergence of simple-cell receptive field properties by learning a sparse code for natural images. *Nature*, 381(6583):607, 1996.
- [30] Anitha Pasupathy. The neural basis of image segmentation in the primate brain. *Neuroscience*, 296:101–109, 2015.
- [31] Mary A Peterson and Bradley S Gibson. Object recognition contributions to figure-ground organization: Operations on outlines and subjective contours. *Perception & Psychophysics*, 56(5):551–564, 1994.
- [32] Jordi Pont-Tuset and Ferran Marques. Measures and meta-measures for the supervised evaluation of image segmentation. In *Proceedings of the IEEE Conference on Computer Vision and Pattern Recognition*, pages 2131–2138, 2013.
- [33] Alexandre Pouget, Jeffrey M Beck, Wei Ji Ma, and Peter E Latham. Probabilistic brains: knowns and unknowns. *Nature neuroscience*, 16(9):1170, 2013.
- [34] Fangtu T Qiu and Rüdiger Von Der Heydt. Figure and ground in the visual cortex: V2 combines stereoscopic cues with gestalt rules. *Neuron*, 47(1):155–166, 2005.
- [35] Carl Edward Rasmussen. The infinite gaussian mixture model. In S. A. Solla, T. K. Leen, and K. Müller, editors, *Advances in Neural Information Processing Systems 12*, pages 554–560. MIT Press, 2000.

- [36] Pieter R Roelfsema. Cortical algorithms for perceptual grouping. *Annu. Rev. Neurosci.*, 29:203–227, 2006.
- [37] Olaf Ronneberger, Philipp Fischer, and Thomas Brox. U-net: Convolutional networks for biomedical image segmentation. In *International Conference on Medical image computing and computer-assisted intervention*, pages 234–241. Springer, 2015.
- [38] Toni P Saarela and Michael S Landy. Combination of texture and color cues in visual segmentation. *Vision research*, 58:59–67, 2012.
- [39] Luis G Sanchez-Giraldo, Md Nasir Uddin Laskar, and Odelia Schwartz. Normalization and pooling in hierarchical models of natural images. *Current opinion in neurobiology*, 55:65–72, 2019.
- [40] Odelia Schwartz, Terrence J. Sejnowski, and Peter Dayan. Soft mixer assignment in a hierarchical generative model of natural scene statistics. *Neural Computation*, 18:2680–2718, 2006.
- [41] Matthew W Self, Danique Jeurissen, Anne F van Ham, Bram van Vugt, Jasper Poort, and Pieter R Roelfsema. The segmentation of proto-objects in the monkey primary visual cortex. *Current Biology*, 2019.
- [42] Giorgos Sfikas, Christophoros Nikou, and Nikolaos Galatsanos. Edge preserving spatially varying mixtures for image segmentation. In *2008 IEEE Conference on Computer Vision and Pattern Recognition*, pages 1–7. IEEE, 2008.
- [43] Mariano Sigman, Guillermo A Cecchi, Charles D Gilbert, and Marcelo O Magnasco. On a common circle: natural scenes and gestalt rules. *Proceedings of the National Academy of Sciences*, 98(4):1935–1940, 2001.
- [44] Karen Simonyan and Andrew Zisserman. Very deep convolutional networks for large-scale image recognition. *arXiv preprint arXiv:1409.1556*, 2014.
- [45] Shiliang Sun, John Paisley, and Qiuyang Liu. Location dependent dirichlet processes. In *International Conference on Intelligent Science and Big Data Engineering*, pages 64–76. Springer, 2017.
- [46] Jonathan Vacher, Pascal Mamassian, and Ruben Coen-Cagli. Probabilistic model of visual segmentation, 2018.
- [47] Aäron van den Oord and Benjamin Schrauwen. Factoring variations in natural images with deep gaussian mixture models. In Zoubin Ghahramani, Max Welling, Corinna Cortes, Neil D. Lawrence, and Kilian Q. Weinberger, editors, *NIPS*, pages 3518–3526, 2014.
- [48] Cinzia Viroli and Geoffrey J. McLachlan. Deep gaussian mixture models. *Statistics and Computing*, 29(1):43–51, 2019.
- [49] Johan Wagemans, James H Elder, Michael Kubovy, Stephen E Palmer, Mary A Peterson, Manish Singh, and Rüdiger von der Heydt. A century of gestalt psychology in visual perception: I. perceptual grouping and figure–ground organization. *Psychological bulletin*, 138(6):1172, 2012.
- [50] Martin J Wainwright and Eero P Simoncelli. Scale mixtures of gaussians and the statistics of natural images. In *Advances in neural information processing systems*, pages 855–861, 2000.
- [51] Thomas SA Wallis, Christina M Funke, Alexander S Ecker, Leon A Gatys, Felix A Wichmann, and Matthias Bethge. A parametric texture model based on deep convolutional features closely matches texture appearance for humans. *Journal of vision*, 17(12):5–5, 2017.
- [52] Xulun Ye, Jieyu Zhao, and Yu Chen. A nonparametric model for multi-manifold clustering with mixture of gaussians and graph consistency. *Entropy*, 20(11):830, 2018.
- [53] Qiyang Zhao. Segmenting natural images with the least effort as humans. In *BMVC*, pages 110–1, 2015.

A Propositions and Proofs

Proposition 2. For all $(n, k) \in \{1, \dots, N\} \times \{1, \dots, K\}$, let $f_{n,k} : \mathbb{R}^N \rightarrow \mathbb{R}$ be any linear function such that $f_{n,k}([0, +\infty[^N) \subset \mathbb{R}_+$. Set $\mathbf{B}_n = (f_{n,1}(\delta_1^C) - \delta_1^{C_n} + 1, \dots, f_{n,K}(\delta_K^C) - \delta_K^{C_n} + 1)$

as the Dirichlet prior parameter. Then, the mixing probability updates are

$$\forall (n, k) \in \{1, \dots, N\} \times \{1, \dots, K\}, \quad p_{n,k}^{(t+1)} = \frac{f_{n,k}(\tau_{\cdot,k}^{(t)})}{\sum_{k=1}^K f_{n,k}(\tau_{\cdot,k}^{(t)})}. \quad (12)$$

where $\tau_{n,k}^{(t)} = \mathbb{P}_{C_n | X_n, \Theta}(k | x_n, \boldsymbol{\theta}^{(t)})$ is the k^{th} component posterior probability of sample x_n at the previous E-step and $\boldsymbol{\theta}^{(t)}$ is the previous parameter estimate.

Proof. Using the Dirichlet prior (2) of the main paper, the completed log-posterior writes

$$\ell(\boldsymbol{\theta}; (x_n, C_n, \mathbf{B}_n)_n) = \sum_{n=1}^N \sum_{k=1}^K (B_{n,k} - 1 + \delta_k^{C_n}) \ln(p_{n,k}) + W((x_n, C_n, \mathbf{B}_n)_n; \boldsymbol{\alpha}),$$

where W is the function that gathers all the terms of ℓ that does not depend on $p_{n,k}$. Knowing the previous parameter estimate $\boldsymbol{\theta}^{(t)}$, the E-step consists in taking the conditional expectation of the log-posterior ℓ which is

$$Q(\boldsymbol{\theta}; \boldsymbol{\theta}^{(t)}, (x_n)_n) = \sum_{n=1}^N \sum_{k=1}^K \mathbb{E} \left(B_{n,k} - 1 + \delta_k^{C_n} | (x_n)_n, \boldsymbol{\theta}^{(t)} \right) \ln(p_{n,k}) + w((x_n)_n; \boldsymbol{\alpha}, \boldsymbol{\theta}^{(t)}),$$

where $w((x_n)_n; \boldsymbol{\alpha}, \boldsymbol{\theta}^{(t)}) = \mathbb{E} (W((x_n, C_n, \mathbf{B}_n)_n; \boldsymbol{\alpha}) | (x_n)_n, \boldsymbol{\theta}^{(t)})$ and

$$\begin{aligned} \mathbb{E} \left(B_{n,k} - 1 + \delta_k^{C_n} | (x_n)_n, \boldsymbol{\theta}^{(t)} \right) &= \mathbb{E} \left(f_{n,k}(\delta_k^{C_n}) | (x_n)_n, \boldsymbol{\theta}^{(t)} \right) \\ &= f_{n,k} \left(\mathbb{E} \left(\delta_k^{C_n} | (x_n)_n, \boldsymbol{\theta}^{(t)} \right) \right) = f_{n,k} \left(\tau_{\cdot,k}^{(t)} \right), \end{aligned}$$

where $\tau_{n,k}^{(t)}$ is defined in the proposition. Then, the M-step consists in maximizing the expected log-posterior Q with respect to $\boldsymbol{\theta} = (\mathbf{p}_n, \boldsymbol{\alpha})$. We only consider optimization with respect to \mathbf{p}_n which is independent from the optimization with respect to $\boldsymbol{\alpha}$. To obtain the update rule for \mathbf{p}_n with first add the Lagrange multiplier associated to the constraint $\sum_k p_{n,k} = 1$ and compute the partial derivative with respect to $p_{n,k}$. Therefore,

$$\forall (n, k) \in \{1, \dots, N\} \times \{1, \dots, K\}, \quad \frac{f_{n,k}(\tau_{\cdot,k}^{(t)})}{p_{n,k}} + \lambda_n = 0,$$

which leads to the update rule (4) by setting λ_n such that $\sum_k p_{n,k} = 1$. \square

Proposition 3. For all $(n, k, h) \in \{1, \dots, N\} \times \{1, \dots, K\} \times \{1, \dots, H\}$, let $f_{n,k}^{(h)} : \mathbb{R}^N \rightarrow \mathbb{R}$ be any linear function such that $f_{n,k}^{(h)}([0, +\infty[^{NH}) \subset \mathbb{R}_+$. Set

$$\mathbf{B}_n^{(h)} = (f_{n,1}^{(h)}(\delta_1^{C_n^{(1)}}, \dots, \delta_1^{C_n^{(H)}}) - \delta_1^{C_n^{(h)}} + 1, \dots, f_{n,K}^{(h)}(\delta_K^{C_n^{(1)}}, \dots, \delta_K^{C_n^{(H)}}) - \delta_K^{C_n^{(h)}} + 1)$$

as the Dirichlet prior parameter. Then, the mixing probability updates of layer h are

$$\begin{aligned} \forall (n, k, h) \in \{1, \dots, N\} \times \{1, \dots, K\} \times \{1, \dots, H\}, \\ p_{n,k}^{(t+1,h)} = \frac{f_{n,k}^{(h)}(\tau_{\cdot,k}^{(t,1)}, \dots, \tau_{\cdot,k}^{(t,H)})}{\sum_{k=1}^K f_{n,k}^{(h)}(\tau_{\cdot,k}^{(t,1)}, \dots, \tau_{\cdot,k}^{(t,H)})}. \end{aligned} \quad (13)$$

where $\tau_{n,k}^{(t,h)} = \mathbb{P}_{C_n^{(h)} | X_n^{(h)}, \Theta}(k | x_n^{(h)}, \boldsymbol{\theta}^{(t,h)})$ is the k^{th} component posterior probability of sample $x_n^{(h)}$ at the previous E-step and $\boldsymbol{\theta}^{(t,h)}$ is the previous parameter estimate.

Proof. The proof is similar to the proof of Proposition 1 and starts by writing the log-posterior of each layers and then taking the conditional expectation knowing all the other features and previous parameter estimations at all layers

$$\begin{aligned} \mathbb{E} \left(B_{n,k}^{(h)} - 1 + \delta_k^{C_n^{(h)}} | (x_n)_n, \boldsymbol{\theta}^{(t)} \right) &= \mathbb{E} \left(f_{n,k}^{(h)} \left(\delta_k^{C_n^{(1)}}, \dots, \delta_k^{C_n^{(H)}} \right) | \left((x_n^{(h)})_n, \boldsymbol{\theta}^{(t,h)} \right)_h \right) \\ &= f_{n,k}^{(h)} \left(\mathbb{E} \left(\left(\delta_k^{C_n^{(1)}}, \dots, \delta_k^{C_n^{(H)}} \right) | \left((x_n^{(h)})_n, \boldsymbol{\theta}^{(t,h)} \right)_h \right) \right) \\ &= f_{n,k}^{(h)}(\tau_{\cdot,k}^{(t,1)}, \dots, \tau_{\cdot,k}^{(t,H)}). \end{aligned}$$

We conclude by using Lagrange multipliers as in the proof of Proposition 1. □

The update rules (6,7,8) of the main paper are obtained by respectively setting $f_{n,k}^{(h)}$ as it follows

$$f_{n,k}^{(h)}(\tau_{\cdot,k}^{(t,1)}, \dots, \tau_{\cdot,k}^{(t,H)}) = \tau_{n,k}^{(h)} + \frac{m_{n,k}^{(h,t)}}{s_n^{(h,t)^2}},$$

$$f_{n,k}^{(h)}(\tau_{\cdot,k}^{(t,1)}, \dots, \tau_{\cdot,k}^{(t,H)}) = \sum_{h=1}^H \frac{m_{n,k}^{(h,t)}}{s_n^{(h,t)^2}},$$

$$f_{n,k}^{(h)}(\tau_{\cdot,k}^{(t,1)}, \dots, \tau_{\cdot,k}^{(t,H)}) = \frac{m_{n,k}^{(h-1,t)}}{s_n^{(h-1,t)^2}} + \frac{m_{n,k}^{(h,t)}}{s_n^{(h,t)^2}} + \frac{m_{n,k}^{(h+1,t)}}{s_n^{(h+1,t)^2}},$$

where $m_{n,k}^{(h,t)}$ and $s_n^{(h,t)^2}$ are function of $\tau_{\cdot,k}^{(t,h)}$ defined by Equations (9,10) of the main paper.

B Additional Figures

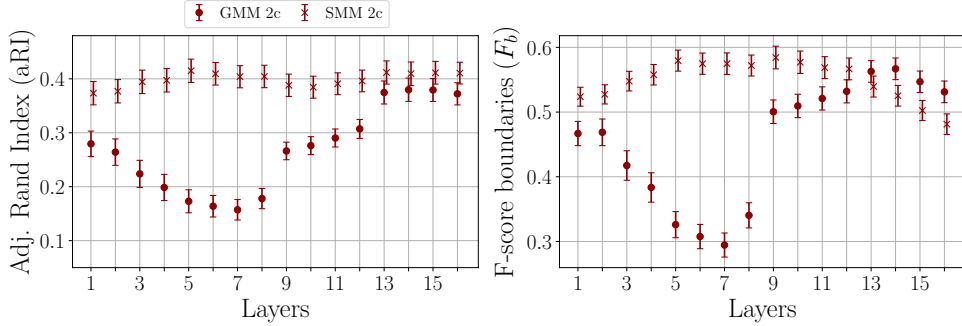


Figure 7: Adjusted Rand Index (aRI) and F-score for boundaries (F_b) for low resolution segmentation maps. All segmentation maps are sub-sampled to the resolution of the deepest layer.

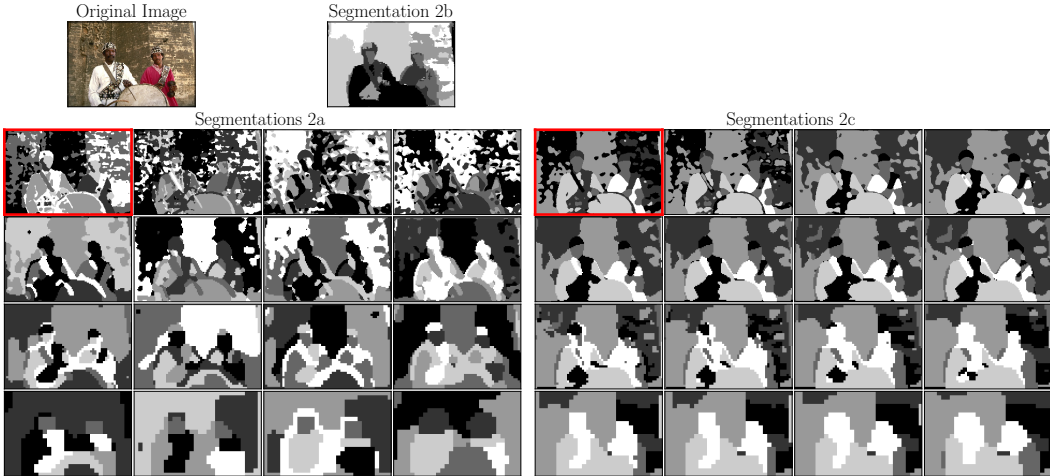


Figure 8: Segmentation maps obtained with Student-t mixtures for the three models. All layers have the same number of components that is used for synthesis (main paper Figure 6). The red frame indicates the best layer (with highest aRI score).

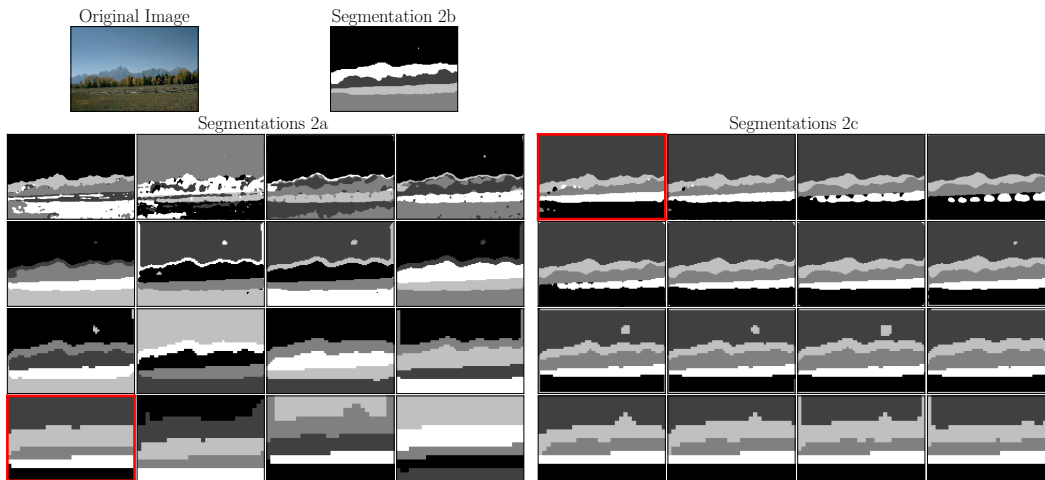


Figure 9: Segmentation maps obtained with Student- t mixtures for the three models. All layers have the same number of components that is used for synthesis (main paper Figure 6). The red frame indicates the best layer (with highest aRI score).

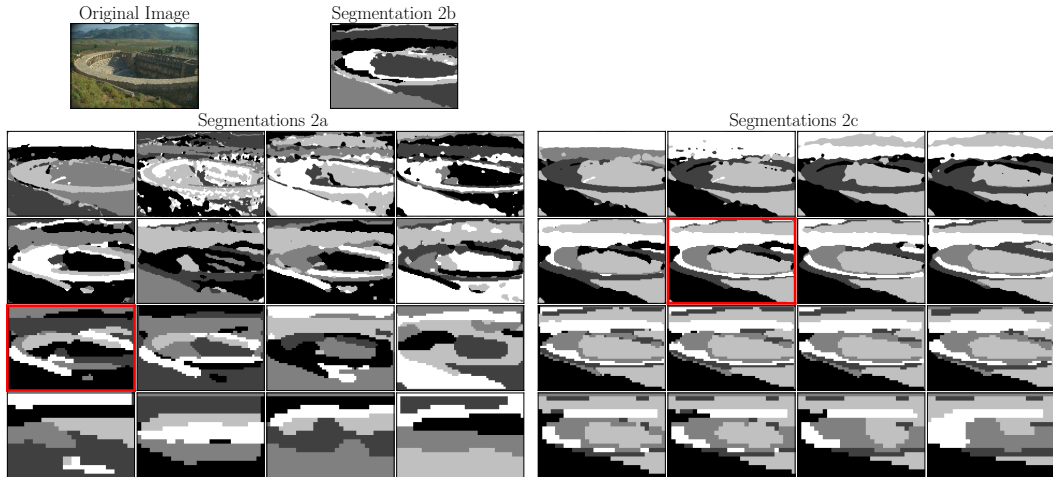


Figure 10: Segmentation maps obtained with Student- t mixtures for the three models. All layers have the same number of components that is used for synthesis (main paper Figure 6). The red frame indicates the best layer (with highest aRI score).

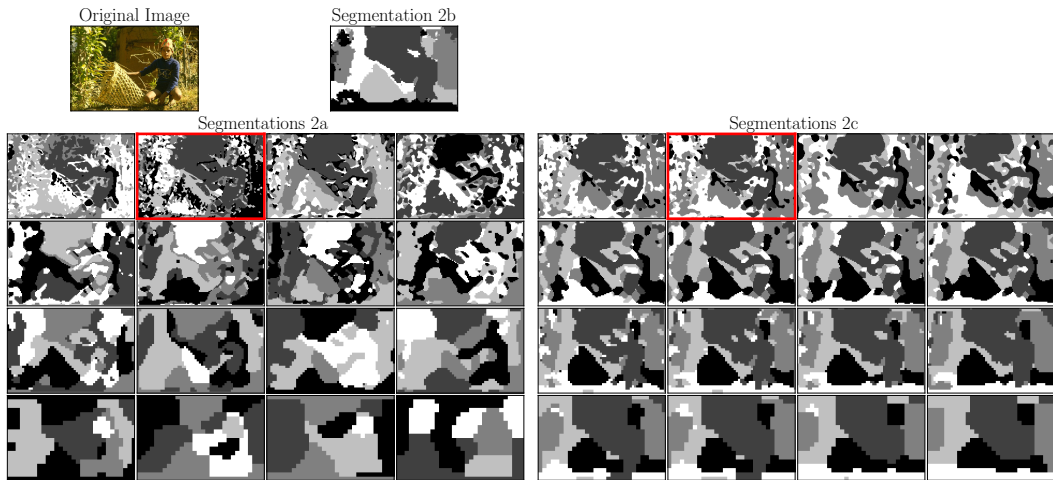


Figure 11: Segmentation maps obtained with Student- t mixtures for the three models. All layers have the same number of components that is used for synthesis (main paper Figure 6). The red frame indicates the best layer (with highest aRI score).

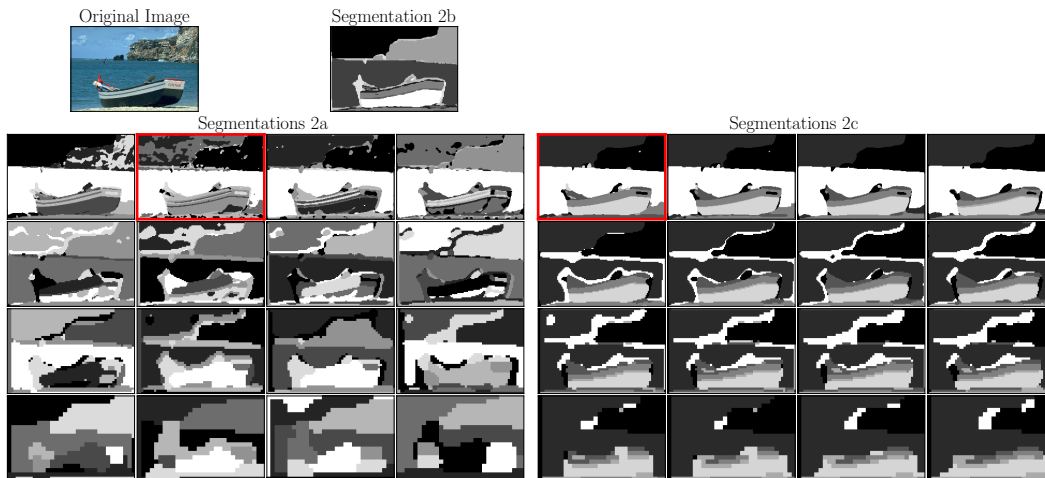


Figure 12: Segmentation maps obtained with Student- t mixtures for the three models. All layers have the same number of components corresponding to the number of components of the best layer. The red frame indicates the best layer (with highest aRI score).

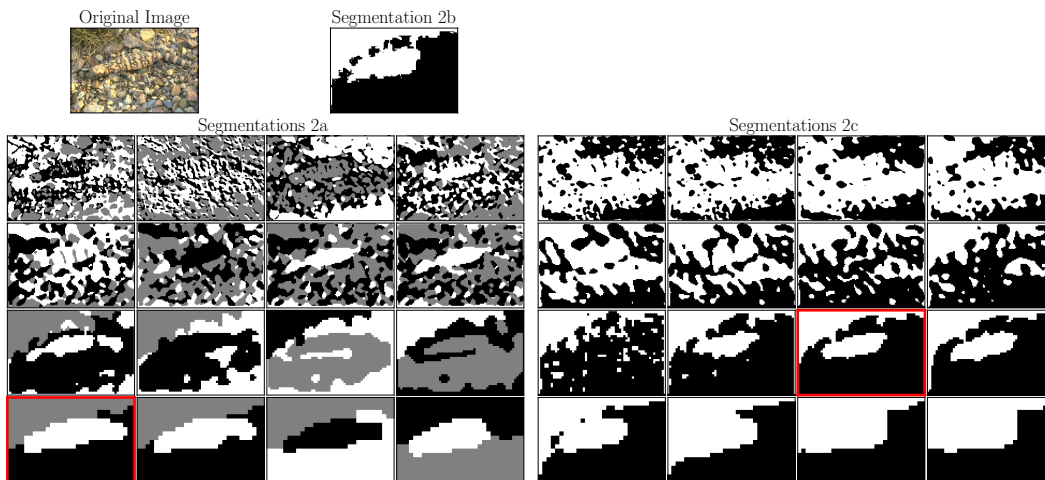


Figure 13: Segmentation maps obtained with Student- t mixtures for the three models. All layers have the same number of components corresponding to the number of components of the best layer. The red frame indicates the best layer (with highest aRI score).

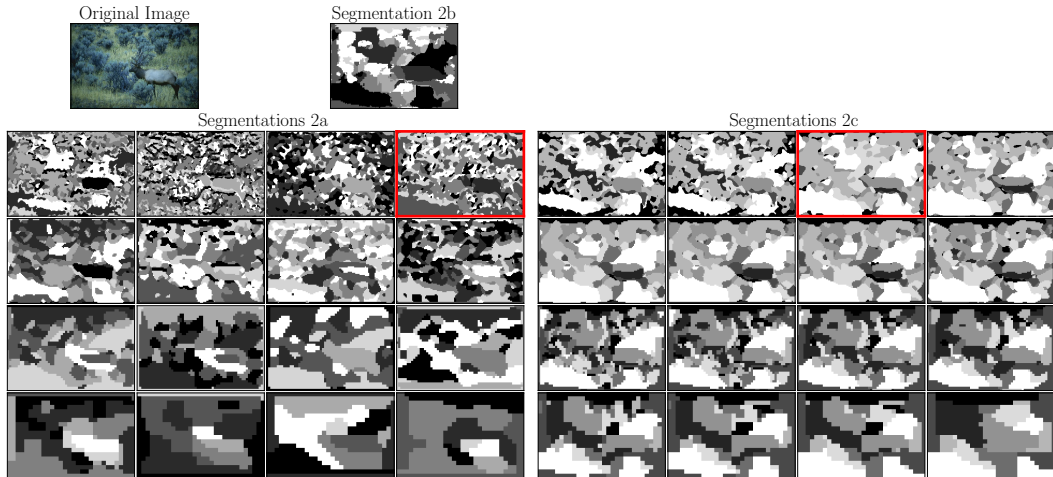


Figure 14: Segmentation maps obtained with Student- t mixtures for the three models. All layers have the same number of components corresponding to the number of components of the best layer. The red frame indicates the best layer (with highest aRI score).

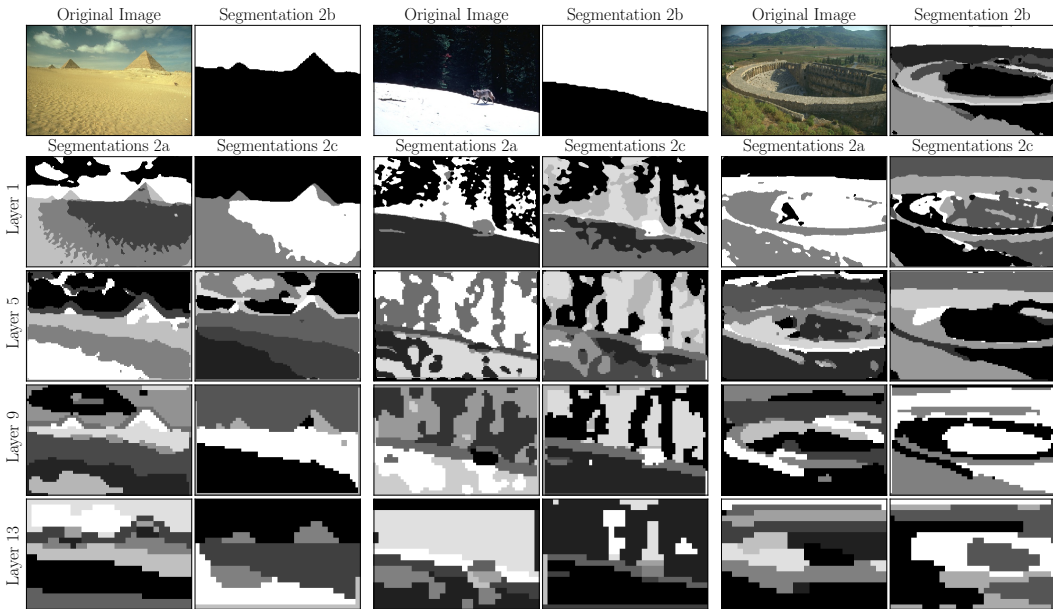


Figure 15: Segmentation maps obtained with Student- t mixtures for the three models. Layers 1, 5, 9 and 13 have the number of components that gives the best aRI score.

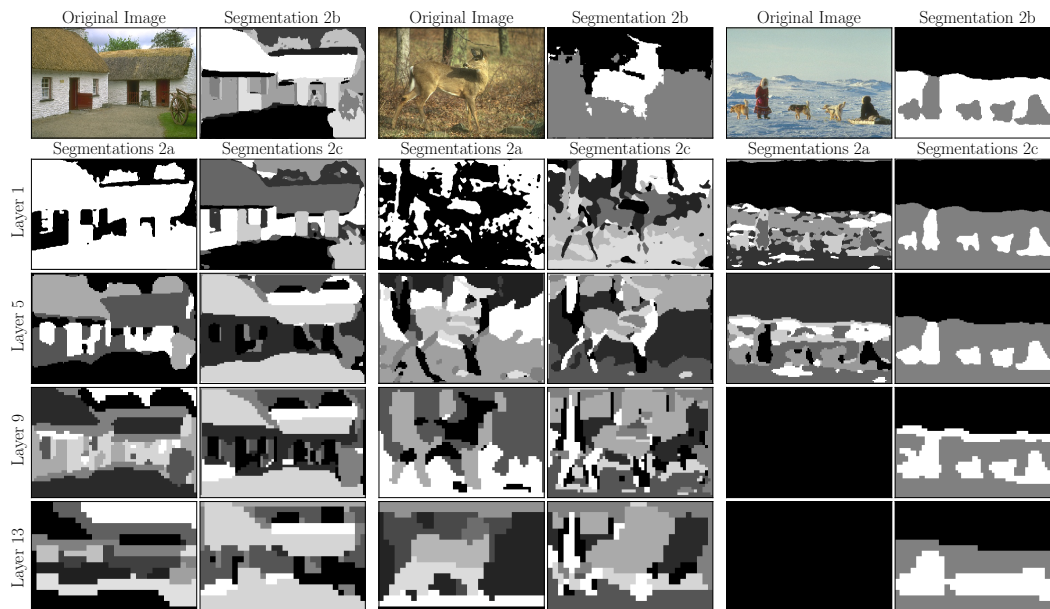


Figure 16: Segmentation maps obtained with Student- t mixtures for the three models. Layers 1, 5, 9 and 13 have the number of components that gives the best aRI score.